Intermetallic Magnesium Compounds $RE_2Ni_2Mg_3$ (RE = Gd, Dy–Tm, Lu) with $Tb_2Ni_2Mg_3$-type Structure

Stefan Linsinger, Matthias Eul, Hamdi Ben Yahia, Manfred H. Möller, and Rainer Pöttgen

Institut für Anorganische und Analytische Chemie, Universität Münster, Corrensstraße 30, 48149 Münster, Germany

Reprint requests to R. Pöttgen. E-mail: pottgen@uni-muenster.de

New intermetallic magnesium compounds $RE_2Ni_2Mg_3$ (RE = Gd, Dy–Tm, Lu) were synthesized from the elements by induction melting. They are isotypic with $Tb_2Ni_2Mg_3$. The structure of $Gd_2Ni_2Mg_3$ was refined from X-ray powder data: $Cmmm$, a = 398.7(1), b = 2121.9(7), c = 368.39(9) pm, R_B = 7.49 %, 3800 data points, 23 parameters. The $RE_2Ni_2Mg_3$ intermetallics are intergrowth variants of AlB_2- and CsCl-related slabs. $Gd_2Ni_2Mg_3$ is a Curie-Weiss paramagnet above 75 K with an experimental magnetic moment of μ_{eff} = 8.16(1) μ_B / Gd atom. Antiferromagnetic ordering sets in at T_N = 42.0(5) K.

Key words: Intermetallics, Magnesium, Crystal Chemistry

Introduction

Intermetallic rare earth (RE) transition metal (T) magnesium compounds $RE_xT_yMg_z$ have intensively been studied in the last years with respect to their technical importance in precipitation hardening in lightweight alloys [1], as well as for their hydrogenation behavior for use as hydrogen storage materials [2, and refs. cited therein]. Since the density of the respective materials is a limiting factor, the RE-T-Mg systems with the lighter and also cheaper 3d metals have preferably been studied with respect to potential applications. Complete or partial phase diagrams have been published for La-Ni-Mg [3, 4], La-Cu-Mg [5], Ce-Ni-Mg [6], Pr-Ni-Mg [7], Nd-Ni-Mg [8], Y-Ni-Mg [9], Y-Cu-Mg [10], and Yb-Cu-Mg [11].

Most structural studies have been performed for the nickel-containing materials. Besides the more complicated structures of $La_{43}Ni_{17}Mg_5$ [12], RE_4NiMg [13 – 16], and $RE_{23}Ni_7Mg_4$ [16, 17], a variety of compounds with supposedly complex structures can be easily described as simple intergrowth variants of well known binary structure types. Considering this principle, we can describe the structures of RE_2Ni_2Mg [18 – 20], TbNiMg [21], $Tb_2Ni_2Mg_3$ [22], and $Tb_{4+x}Ni_2Mg_{3-x}$ [21] as intergrowth variants of AlB_2, α-Fe, and CsCl slabs. The $RENi_9Mg_2$ phases [23] are stacking variants of $CaCu_5$- and $MgNi_2$-related slabs.

In the course of our systematic studies of such magnesium-based intergrowth structures we obtained a whole series of compounds $RE_2Ni_2Mg_3$ (RE = Gd, Dy–Tm, Lu) which are isotypic with $Tb_2Ni_2Mg_3$ [22]. The synthesis and the structural and magnetic characterization of these new intermetallic compounds are reported herein.

Experimental Section

Synthesis

Starting materials for the preparation of the $RE_2Ni_2Mg_3$ samples were ingots of the rare earth metals (Johnson Matthey and Smart Elements, > 99.9 %), nickel powder (Merck, > 99.9 %) and a magnesium rod (Alpha Aesar, > 99.8 %, the surface layer of the rod was removed on a turning lathe). The rare earth metal ingots were first cut into smaller pieces and arc-melted [24] to small buttons under an argon atmosphere. The argon was purified with titanium sponge (900 K), silica gel, and molecular sieves.

The rare earth metal buttons were then added to the nickel powder and the pieces of the magnesium rod in the appropriate amounts and sealed in small tantalum ampoules under an argon pressure of *ca.* 700 mbar. The ampoules were placed in a water-cooled sample chamber of a high-frequency furnace (Hüttinger Elektronik, Freiburg, type TIG 1.5/300) under flowing argon [25], heated at about 1370 K and kept at that temperature for 30 min. After the tubes were quenched to r. t. by switching off the power supply, the samples were broken off the tubes (no reaction with the container material

Compound	a (pm)	b (pm)	c (pm)	V (nm^3)	Reference
$Gd_2Ni_2Mg_3$	398.7(1)	2121.9(7)	368.39(9)	0.3117	this work
$Tb_2Ni_2Mg_3$	397.88(7)	2120.3(4)	365.83(7)	0.3086	[22]
$Dy_2Ni_2Mg_3$	396.1(2)	2113.9(6)	362.9(1)	0.3039	this work
$Ho_2Ni_2Mg_3$	393.9(2)	2110.5(9)	360.7(2)	0.2999	this work
$Er_2Ni_2Mg_3$	391.4(2)	2105.6(7)	359.8(2)	0.2965	this work
$Tm_2Ni_2Mg_3$	389.9(3)	2102.7(9)	359.0(1)	0.2943	this work
$Lu_2Ni_2Mg_3$	388.7(2)	2101.9(7)	358.4(2)	0.2928	this work

Table 1. Lattice parameters (Guinier powder data) of the $RE_2Ni_2Mg_3$ samples, space group *Cmmm*, Z = 2.

was observed). The crushed products were then finely ground to powders in an agate mortar, cold-pressed to small pellets (∅ 6 mm) and sealed in evacuated tantalum ampoules. These were sealed in evacuated silica tubes and annealed at 670 K in a muffle furnace for 4 weeks. The resulting dark-grey samples are stable in air. The $RE_2Ni_2Mg_3$ compounds could only be obtained with the rare earth elements from gadolinium to lutetium. With the larger rare earth elements (La–Nd, Sm) mainly the RE_2Ni_2Mg [20] phases resulted under these reaction conditions. Although different annealing sequences were tested for the $RE_2Ni_2Mg_3$ samples, only polycrystalline material was obtained under our conditions.

EDX data

The bulk samples were studied by energy dispersive analyses of X-rays (EDX) using a Zeiss EVO MA10 scanning electron microscope with REF_3, Ni and MgO as standards. Pieces of the bulk samples were previously embedded in methylmetacrylate matrices, and the surface was polished with different silica and diamond pastes. The surface remained unetched for the EDX measurements. No impurity elements heavier than beryllium (detection limit of the instrument) were observed. The compositions determined semi-quantitatively by EDX were in good agreement with the ideal 2 : 2 : 3 composition.

X-Ray diffraction

The polycrystalline samples were characterized by Guinier powder patterns (Cu$K_{\alpha 1}$ radiation, α-quartz: a = 491.30, c = 540.46 pm as internal standard). The Guinier camera was equipped with an imaging plate device (Fujifilm, BAS-READER 1800). The orthorhombic lattice parameters (Table 1) were obtained through least-squares refinements. The correct indexing was ensured by comparison of the experimental patterns with calculated ones [26].

To refine the crystal structure of $Gd_2Ni_2Mg_3$, a high-precision X-ray powder diffraction measurement was performed. The data were collected at r. t. over the 2θ angle range $2° \leq 2\theta \leq 40°$ with a step size of 0.1° (120 s per step; 4 separate data collection ranges were added up) using a STOE Stadi P diffractometer operating with Mo$K_{\alpha 1}$ radiation (λ = 0.71069 Å).

Table 2. Crystal data and structure refinement for $Gd_2Ni_2Mg_3$.

Compound	$Gd_2Ni_2Mg_3$
Structure type	$Tb_2Ni_2Mg_3$
Space group; Z	*Cmmm*; 2
Lattice parameters	Table 1
Molar mass, g mol^{-1}	504.87
Calculated density, g cm^{-3}	5.38
Absorption coefficient, mm^{-1}	27.1
$F(000)$, e	440
θ range; increment, deg	2 – 39.99; 0.1
Exposure time per step, s	120
Number of data points	3800
Total no. reflections	108
Parameters	23
R_p	0.0553
R_{wp}	0.0698
R_{exp}	0.0692
R_B	0.0749
χ^2	1.01

Structure refinement

The X-ray powder diffraction pattern of $Gd_2Ni_2Mg_3$ was indexed on the basis of an orthorhombic unit cell, a = 398.7(1), b = 2121.9(7), c = 368.39(9) pm. The observed systematic extinctions are compatible with the space group *Cmmm*, in good agreement with the previous work
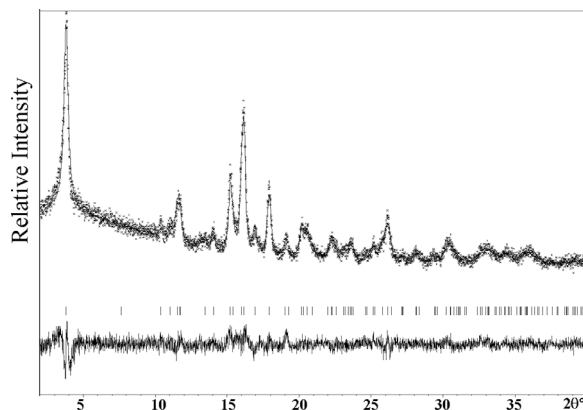

Fig. 1. Observed (crosses) and calculated (solid line) powder pattern of $Gd_2Ni_2Mg_3$ after Rietveld refinement. The tick marks indicate the reflection positions, and the difference plot is shown below.

Table 3. Atom positions and isotropic displacement parameters (Å^2) for $Gd_2Ni_2Mg_3$ The Mg1 and Mg2 sites were refined with contrained APD's.

Atom	Wyckoff site	x	y	z	U_{iso}
Gd	4i	0	0.1753(2)	0	0.0101(14)
Ni	4j	0	0.2899(6)	1/2	0.021(3)
Mg1	4j	0	0.4154(12)	1/2	0.004(5)
Mg2	2a	0	0	0	0.004(5)

Table 4. Interatomic distances (pm) for $Gd_2Ni_2Mg_3$. All distances within the first coordination spheres are listed. Standard deviations are equal or smaller than 1.5 pm.

Gd:	4	Ni	281.3	Mg1:	1	Ni	266.3
	2	Ni	305.1		4	Mg2	325.4
	4	Mg1	332.7		4	Gd	332.7
	2	Gd	368.4		1	Mg1	359.0
	1	Mg2	372.0		2	Mg1	368.4
	2	Gd	374.5	Mg2:	8	Mg1	325.4
	2	Gd	398.7		2	Mg2	368.4
Ni:	2	Ni	261.6		2	Gd	372.0
	1	Mg1	266.3				
	4	Gd	281.3				
	2	Gd	305.1				

on $Tb_2Ni_2Mg_3$ (*Cmmm*, a = 397.88(7), b = 2120.3(4), c = 365.83(7) pm) [22]. The atomic positions of $Tb_2Ni_2Mg_3$ [22] were used as a starting model for the Rietveld analysis using the JANA2006 program package [27]. The background was estimated by a Legendre function, and the peak shapes were described by a pseudo-Voigt function. Data collection and evaluation parameters are listed in Table 2.

After refinement of all atomic positions with isotropic atomic displacement parameters (ADP), the profile factors converged to the values R_p / R_{wp} = 5.88 / 7.43 % and R_B = 8.74. In the final stage of the refinement a preferential orientation (March-Dollase function) along the (010) direction was taken into account and improved the reliability factors to R_p / R_{wp} = 5.53 / 6.98 % and R_B = 7.49 %, however, a negative ADP value was observed for Mg1. Therefore, the Mg1 and Mg2 sites were restricted to have the same ADP. Fig. 1 shows the agreement between the calculated and observed profiles for $Gd_2Ni_2Mg_3$. The refined positional parameters and interatomic distances are listed in Tables 3 and 4.

Further details of the crystal structure investigation may be obtained from Fachinformationszentrum Karlsruhe, 76344 Eggenstein-Leopoldshafen, Germany (fax: +49-7247-808-666; e-mail: crysdata@fiz-karlsruhe.de, http://www.fiz-informationsdienste.de/en/DB/icsd/depot_anforderung.html) on quoting the deposition number CSD-421933.

Magnetic data

10.254 mg of the $Gd_2Ni_2Mg_3$ sample were packed in kapton foil and attached to a sample holder rod. The magnetic properties were measured using the VSM-Option in a Quan-

tum Design Physical-Property-Measurement-System in the temperature range 2.1 – 305 K with magnetic flux densities up to 80 kOe.

Discussion

Crystal chemistry

The $RE_2Ni_2Mg_3$ (RE = Gd, Dy–Tm, Lu) compounds are isotypic with the recently reported compound $Tb_2Ni_2Mg_3$ [22]. The cell volume (Table 1) decreases from the gadolinium to the lutetium compound as expected from the lanthanoid contraction. A projection of the $Gd_2Ni_2Mg_3$ structure onto the xy plane is presented in Fig. 2. Similar to the series of RE_2Ni_2Mg compounds [20], the $RE_2Ni_2Mg_3$ intermetallics are also intergrowth variants of slightly distorted AlB_2- and CsCl-related slabs, but with a slightly different connectivity scheme. The Mg2 atoms have eight Mg1 neighbors (a distorted *bcc* slab), while the distorted cube around Mg1 is formed by four gadolinium and four Mg2 atoms. In the RE_2Ni_2Mg compounds only MgRE_8 cubes occur. An overview on further intergrowth structures with AlB_2- and CsCl-related slabs is given in [22].

Within the condensed trigonal prisms of the AlB_2 slabs the Ni-Ni zig-zag chains show Ni–Ni distances of 262 pm, slightly longer than in *fcc* nickel (249 pm) [28]. This is also the case in the RE_2Ni_2Mg com-
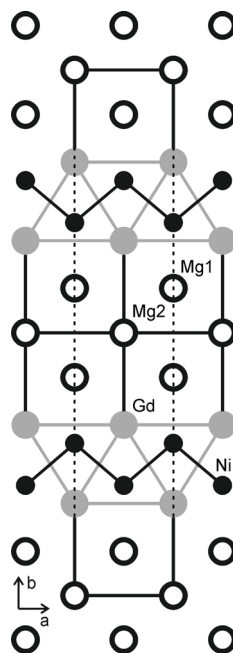

Fig. 2. Projection of the $Gd_2Ni_2Mg_3$ structure onto the xy plane. The AlB_2- and CsCl-related slabs are emphasized.

pounds which contain Ni_2 dumb-bells, *e. g.* 255 pm in Gd_2Ni_2Mg [29]. The Ni-Ni zig-zag chains connect to the Mg1 atoms at a Ni–Mg1 distance of 266 pm, and to four nearest gadolinium neighbors at Ni–Gd of 281 pm. These Ni–Gd distances are close to the sum of the covalent radii [30] of 276 pm, indicating substantial Ni–Gd bonding. In Gd_2Ni_2Mg [29] the Ni–Mg distances of 296 pm are much longer, and most likely a constraint imposed by the different connectivities of the AlB_2- and CsCl-related slabs.

While we observe isolated magnesium atoms in Gd_2Ni_2Mg [29], insertion of further magnesium atoms into $Gd_2Ni_2Mg_3$ leads to a pronounced magnesium substructure. Within the double layer of CsCl-related slabs we observe aggregation of the magnesium atoms leading to $Mg2Mg1_8$ cubes. The Mg2–Mg1 distances of 325 pm are only slightly longer than the average Mg–Mg distance of 320 pm in *hcp* magnesium [28]. This is a quite peculiar magnesium substructure. Similar *bcc* related magnesium slabs also occur in the structures of $LaCuMg_4$ (310–324 pm) and $TbCuMg_4$ (311–335 pm) [31]. Another interesting three-dimensional magnesium substructure is found in the lonsdaleite-related network of slightly puckered hexagons in $LaNiMg_2$ (303–331 pm) [32], while isolated Mg_4 tetrahedra occur in the rare earth metal-rich compounds Gd_4NiMg (309 pm) [13] and $La_{23}Ni_7Mg_4$ (319 pm) [17]. These structural features very much resemble the crystal chemistry of intermetallic $RE_xT_yIn_z$ indides [33]. Since only few of the *RE-T*-Mg phase diagrams have been explored so far, we can expect further interesting intermetallics in these systems.

Magnetic properties

The gadolinium compound was obtained in X-ray-pure form. The temperature dependence of the magnetic and reciprocal magnetic susceptibility of $Gd_2Ni_2Mg_3$ is displayed in Fig. 3. The inverse magnetic susceptibility (χ^{-1} data) displays a linear dependence of the temperature above 75 K, and antiferromagnetic ordering is observed at low temperature. Fitting of the χ^{-1} data in the range of 75–300 K, using the Curie-Weiss law, leads to an effective magnetic moment $\mu_{eff} = 8.16(1)$ μ_B/Gd atom and a Weiss constant $\theta_p = 23.4(1)$ K, indicating ferromagnetic interactions. The resulting effective magnetic moment is somewhat higher than the value for a free Gd^{3+} ion
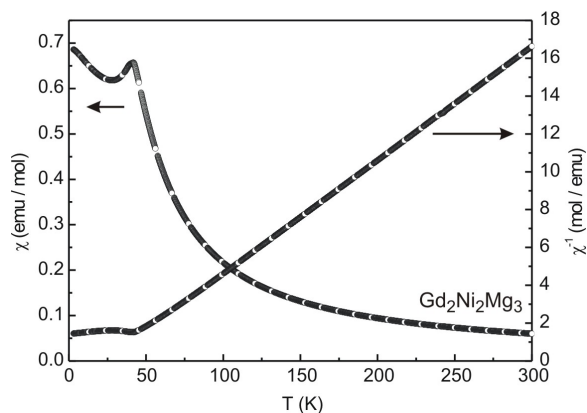

Fig. 3. Temperature dependence of the magnetic susceptibility (χ and χ^{-1} data) of $Gd_2Ni_2Mg_3$ measured at 10 kOe.
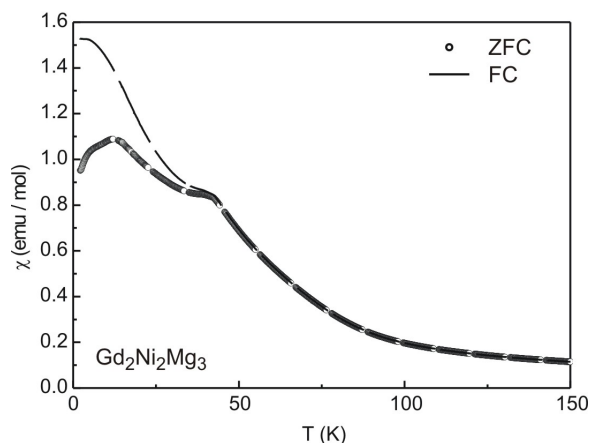

Fig. 4. Low-field susceptibility of $Gd_2Ni_2Mg_3$ measured in the range of 2.1–150 K in a zero-field-cooled and field-cooled state in an external field of 100 Oe.
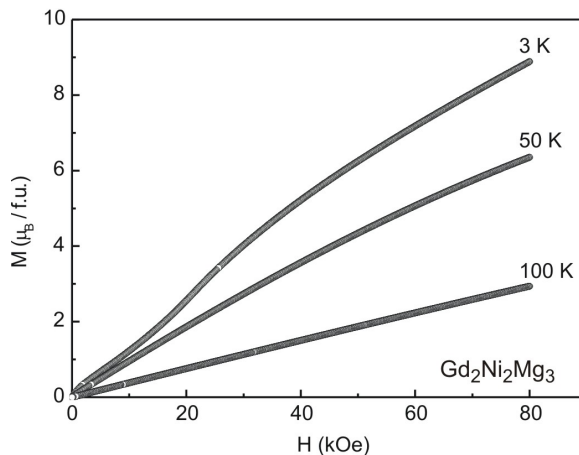

Fig. 5. Magnetization isotherms of $Gd_2Ni_2Mg_3$ measured at 3, 50 and 100 K.

(7.94 μ_B), which can be explained by a contribution from the *d* electrons of gadolinium as already seen in various other intermetallic gadolinium compounds, *e. g.* GdAgMg and GdPtMg [34].

For a precise determination of the Néel temperature a susceptibility measurement in the zero-field-cooled and field-cooled mode in a small field of 100 Oe was performed (Fig. 4). From the kink-point measurement the ordering temperature was determined at T_N = 42.0(5) K, slightly smaller than for the 49 K antiferromagnet Gd_2Ni_2Mg [29]. It should be noted here that the magnetic susceptibility increases at temperatures below T_N in a small as well as in a large external field.

The magnetization isotherms taken at 3, 50, and 100 K are shown in Fig. 5. At 100 K a linear increase of the magnetization with the applied field can be observed, as is expected for a paramagnetic material. At 50 K a slight curvature can be seen, which becomes more pronounced at 3 K. At this temperature a weak metamagnetic step is found at around 20 kOe, but no hysteresis is observed. The metamagnetic step clearly confirms the antiferromagnetic ground state in $Gd_2Ni_2Mg_3$.

[1] K. U. Kainer (Ed.), *Magnesium*, Proceedings of the 6th International Conference on Magnesium Alloys and their Applications, Wiley-VCH, Weinheim **2004**.

[2] U. Ch. Rodewald, B. Chevalier, R. Pöttgen, *J. Solid State Chem.* **2007**, *180*, 1720.

[3] S. De Negri, M. Giovannini, A. Saccone, *J. Alloys Compd.* **2005**, *397*, 126.

[4] S. De Negri, M. Giovannini, A. Saccone, *J. Alloys Compd.* **2007**, *439*, 109.

[5] S. De Negri, M. Giovannini, A. Saccone, *J. Alloys Compd.* **2007**, *427*, 134.

[6] H. Zhou, Y. Wang, Q. Yao, *J. Alloys Compd.* **2006**, *407*, 129.

[7] Z. Huaiying, X. Xin, C. Gang, W. Zhongmin, Z. Songli, *J. Alloys Compd.* **2005**, *386*, 144.

[8] H. Zhou, S. Zhang, Q. Yao, W. Li, *J. Alloys Compd.* **2007**, *429*, 116.

[9] Q. Yao, H. Zhou, Z. Wang, *J. Alloys Compd.* **2006**, *421*, 117.

[10] S. De Negri, P. Solokha, A. Saccone, V. Pavlyuk, *Intermetallics* **2009**, *17*, 614.

[11] S. De Negri, A. Saccone, P. Rogl, G. Giester, *Intermetallics* **2008**, *16*, 1285.

[12] P. Solokha, S. De Negri, V. Pavlyuk, A. Saccone, *Inorg. Chem.* **2009**, *48*, 11586.

[13] S. Tuncel, J. G. Roquefère, C. Stan, J.-L. Bobet, B. Chevalier, E. Gaudin, R.-D. Hoffmann, U. Ch. Rodewald, R. Pöttgen, *J. Solid State Chem.* **2009**, *182*, 229.

[14] S. Linsinger, W. Hermes, B. Chevalier, S. Couillaud, J.-L. Bobet, M. Eul, R. Pöttgen, *Intermetallics* **2009**, *17*, 1028.

[15] S. Couillaud, S. Linsinger, C. Duée, A. Rougier, B. Chevalier, R. Pöttgen, J.-L. Bobet, *Intermetallics* **2010**, *18*, 1115.

[16] P. Solokha, S. De Negri, V. Pavlyuk, A. Saccone, *Chem. Met. Alloys* **2009**, *2*, 39.

[17] S. Tuncel, W. Hermes, B. Chevalier, U. Ch. Rodewald, R. Pöttgen, *Z. Anorg. Allg. Chem.* **2008**, *634*, 2140.

[18] C. Geibel, U. Klinger, M. Weiden, B. Buschinger, F. Steglich, *Physica B* **1997**, *237–238*, 202.

[19] R. Pöttgen, A. Fugmann, R.-D. Hoffmann, U. Ch. Rodewald, D. Niepmann, *Z. Naturforsch.* **2000**, *55b*, 155.

[20] R.-D. Hoffmann, A. Fugmann, U. Ch. Rodewald, R. Pöttgen, *Z. Anorg. Allg. Chem.* **2000**, *626*, 1733.

[21] P. Solokha, S. De Negri, V. Pavlyuk, A. Saccone, *Intermetallics* **2010**, *18*, 719.

[22] P. Solokha, S. De Negri, A. Saccone, V. Pavlyuk, B. Marciniak, J.-C. Tedenac, *Acta Crystallogr.* **2007**, *63C*, i13.

[23] K. Kadir, T. Sakai, I. Uehara, *J. Alloys Compd.* **1997**, *257*, 115.

[24] R. Pöttgen, Th. Gulden, A. Simon, *GIT Labor-Fachzeitschrift* **1999**, *43*, 133.

[25] R. Pöttgen, A. Lang, R.-D. Hoffmann, B. Künnen, G. Kotzyba, R. Müllmann, B. D. Mosel, C. Rosenhahn, *Z. Kristallogr.* **1999**, *214*, 143.

[26] K. Yvon, W. Jeitschko, E. Parthé, *J. Appl. Crystallogr.* **1977**, *10*, 73.

[27] V. Petříček, M. Dušek, L. Palatinus, JANA2006, The Crystallographic Computing System, Institute of Physics, University of Prague, Prague (Czech Republic) **2006**.

[28] J. Donohue, *The Structures of the Elements*, Wiley, New York **1974**.

[29] K. Łątka, R. Kmieć, A. W. Pacyna, R. Mishra, R. Pöttgen, *Solid State Sci.* **2001**, *3*, 545.

[30] J. Emsley, *The Elements*, Oxford University Press, Oxford **1999**.

[31] P. Solokha, S. De Negri, V. Pavlyuk, A. Saccone, B. Marciniak, *J. Solid State Chem.* **2007**, *180*, 3066.

[32] G. Renaudin, L. Guénée, K. Yvon, *J. Alloys Compd.* **2003**, *145*, 350.

[33] Ya. M. Kalychak, V. I. Zaremba, R. Pöttgen, M. Lukachuk, R.-D. Hoffmann, Rare Earth-Transition Metal-Indides in *Handbook on the Physics and Chemistry of Rare Earths*, (Eds.: K. A. Gschneider, Jr., V. K. Pecharsky, J.-C. Bünzli), Vol. 34, Elsevier, Amsterdam, **2005**, chapter 218, pp. 1.

[34] K. Łątka, R. Kmieć, A. W. Pacyna, T. Tomkowicz, R. Mishra, T. Fickenscher, H. Piotrowski, R.-D. Hoffmann, R. Pöttgen, *J. Solid State Chem.* **2002**, *168*, 331.